SECURITY INFORMATION

[redacted]

Copy 214
RM L52D24a

NACA RM L52D24a

TECH LIBRARY KAFB, NM
0144454

[redacted]

NACA

RESEARCH MEMORANDUM

73328

LONGITUDINAL STABILITY AND CONTROL CHARACTERISTICS FROM A FLIGHT INVESTIGATION OF A CRUCIFORM CANARD MISSILE CONFIGURATION HAVING AN EXPOSED WING-CANARD AREA RATIO OF 16:1

By Martin T. Moul and Andrew R. Wineman

Langley Aeronautical Laboratory
Langley Field, Va.

CLASSIFIED DOCUMENT

[redacted]

NATIONAL ADVISORY COMMITTEE
FOR AERONAUTICS
WASHINGTON
June 25, 1952

Receipt signature required

PERMANENT RECORD

[redacted]

Classification cancelled (or changed to Unclassified)

By Authority of Nasa Tech Pub Announcement #99
(OFFICER AUTHORIZED TO CHANGE)

By ..... 13 Apr 56

AND

MK

(GRADE OF OFFICER MAKING CHANGE)

6 Apr 61

DATE

CLASSIFIED

FROM:

TO:

TECH LIBRARY KAFB, NM
0144454

NATIONAL ADVISORY COMMITTEE FOR AERONAUTICS

RESEARCH MEMORANDUM

LONGITUDINAL STABILITY AND CONTROL CHARACTERISTICS FROM A FLIGHT INVESTIGATION OF A CRUCIFORM CANARD MISSILE CONFIGURATION HAVING AN EXPOSED WING-CANARD AREA RATIO OF 16:1

By Martin T. Moul and Andrew R. Wineman

SUMMARY

A flight investigation has been made to determine the longitudinal stability and control characteristics of a 60° delta-wing-canard missile configuration with an exposed wing-canard area ratio of 16:1. The results presented include the longitudinal stability derivatives, control effectiveness, and drag characteristics for a Mach number range of 0.75 to 1.80 and are compared with the results of a similar configuration having larger controls. Stability characteristics are also presented from the flights of an interdigitated canard configuration at a Mach number of 2.08 and a wing-body configuration at Mach numbers of 1.25 to 1.45.

The stability derivatives varied gradually with Mach number with the exception of the damping-in-pitch derivative. Aerodynamic damping in pitch decreased to a minimum at a Mach number of 1.03, then increased to a peak value at a Mach number of 1.26 followed by a gradual decrease at higher Mach numbers. The aerodynamic-center location of the in-line canard configuration shifted rearward 13 percent of the mean aerodynamic chord at transonic speeds. The pitching-moment curve slope was 25 percent greater for the model having no canards than for the in-line configuration. No large effects of interdigitation were noted in the stability derivatives. Pitching effectiveness of the in-line configuration was maintained throughout the Mach number range.

A comparison of the stability and control characteristics of two canard configurations having different area controls showed that decreasing the control area 44 percent decreased the pitching effectiveness proportionally, shifted the aerodynamic-center location rearward 9 to 14 percent of the mean aerodynamic chord, and reduced the total hinge moments required for 1° trimmed flight about 50 percent at transonic speeds.

NA7B-1148

INTRODUCTION

As part of the general research program on the aerodynamics of missiles, the Langley Pilotless Aircraft Research Division has been conducting a series of flight tests to determine the longitudinal stability and control characteristics of a canard missile configuration. The present paper includes results from three models which were tested to determine the effect of wing-canard area ratio and interdigitation upon lift effectiveness, static and dynamic stability, and control effectiveness. The results of a flight investigation of a delta-wing-canard configuration with an exposed wing-canard area ratio of 9:1 was reported in reference 1. The effect of tail length on the stability and control characteristics was reported in reference 2.

Longitudinal stability, control, and drag characteristics of model 1, an in-line canard configuration with an exposed wing-canard area ratio of 16:1, are presented for a Mach number range of 0.75 to 1.80. Model 2, a canard configuration with wings interdigitated (revolved about body axis) 45°, and model 3, a wing-body configuration, were partially successful. The available data from the flights of model 2 at a Mach number of 2.08 and model 3 at Mach numbers of 1.25 to 1.45 are presented.

The models were disturbed in pitch by a programmed square-wave deflection of the canard controls in models 1 and 2 and by the programmed firing of NACA short-duration pulse rockets in model 3. All three models were flight-tested at the Langley Pilotless Aircraft Research Station at Wallops Island, Va.

SYMBOLS

c	wing chord, ft
$\bar{c}$	wing mean aerodynamic chord, ft
S_w	total wing area in one plane, sq ft
$\bar{c}_e$	canard control-surface mean aerodynamic chord, in.
S_e	canard control-surface exposed area, sq ft
t	wing thickness, in.
W	weight, lb

I_y	moment of inertia about Y-axis, slug-ft^2
g	acceleration due to gravity, ft/sec^2
ρ	mass density of air, slugs/cu ft
μ	coefficient of viscosity, slugs/ft-sec
V	velocity of model, ft/sec
V_c	speed of sound in air, ft/sec
M	Mach number, V/V_c
R	Reynolds number, $\rho V\bar{c}/\mu$
q	dynamic pressure, $1/2\rho V^2$, lb/sq ft, or pitching velocity, radians per second
P	period, sec
b	exponential damping coefficient in e^{-bt}, per sec
$T_{1/2}$	time required for oscillations to damp to one-half amplitude, 0.693/b, sec
a_n/g	normal accelerometer reading, g units
a_l/g	longitudinal accelerometer reading, deceleration positive, g units
α	angle of attack, deg
$\dot{\alpha} = \frac{1}{57.3}\frac{d\alpha}{dt}$	radians per sec
δ	canard control deflection, deg
H	hinge moment, in.-lb
C_L	lift coefficient, $\left(\frac{a_n}{g}\cos\alpha - \frac{a_l}{g}\sin\alpha\right)\frac{W}{qS_w}$
C_D	drag coefficient, $\left(\frac{a_l}{g}\cos\alpha + \frac{a_n}{g}\sin\alpha\right)\frac{W}{qS_w}$

C_m pitching-moment coefficient, $\dfrac{\text{Pitching moment about center of gravity}}{qS_w\bar{c}}$

C_h hinge-moment coefficient, $\dfrac{H}{qS_e\bar{c}_e}$

$C_{L_{trim}}$ trim lift coefficient

α_{trim} trim angle of attack, deg

$C_{D_{min}}$ minimum drag coefficient

$(L/D)_{max}$ maximum lift-drag ratio

$\dfrac{dC_D}{dC_L^2}$ drag due to lift

$\dfrac{\Delta H}{\Delta\alpha}$ hinge moment required per degree trim angle of attack, in.-lb/deg

ω angular forcing frequency, radians per sec

$\dfrac{\alpha}{\delta}$ amplitude ratio

φ phase angle, deg

Derivatives:

$C_{L_\alpha} = \dfrac{\partial C_L}{\partial\alpha}$; $C_{m_\alpha} = \dfrac{\partial C_m}{\partial\alpha}$; $C_{h_\alpha} = \dfrac{\partial C_h}{\partial\alpha}$; per deg

$C_{L_\delta} = \dfrac{\partial C_L}{\partial\delta}$; $C_{m_\delta} = \dfrac{\partial C_m}{\partial\delta}$; $C_{h_\delta} = \dfrac{\partial C_h}{\partial\delta}$; per deg

$C_{m_q} = \dfrac{\partial C_m}{\partial\,\dfrac{q\bar{c}}{2V}}$; $C_{m_{\dot{\alpha}}} = \dfrac{\partial C_m}{\partial\,\dfrac{\dot{\alpha}\bar{c}}{2V}}$; per radian

$H_\alpha = \dfrac{\partial H}{\partial\alpha}$; $H_\delta = \dfrac{\partial H}{\partial\delta}$; in.-lb/deg

DESCRIPTION OF THE MODELS

The three models tested had identical fuselages, wings, and longitudinal location of the wings. The fuselage consisted of a 7-inch-diameter cylindrical section with nose and tail cones of a modified Ferri model no. 9 section. The over-all body fineness ratio was 16.3. Delta wings were mounted on the fuselages in a cruciform arrangement. Small fins were mounted on the fuselages near the nose of models 1 and 2 as all-movable control surfaces. On model 1 the control fins and the horizontal wing were in-line and on model 2, the wings were interdigitated (revolved about body axis) 45° with respect to the controls. Model 3 had no control surfaces. Three-view sketches of the three configurations are shown in figure 1.

The solid magnesium wings were flat plates with beveled leading and trailing edges and a 60° delta plan form. The thickness ratio at the root chord was 3 percent. The control fins were steel and had the same plan form and section as the wings. The ratio of wing exposed area to control exposed area was 16:1. Details of the wing and control surface are presented in figure 2. Photographs of the interdigitated model and the canard control surfaces are presented in figure 3.

The models were boosted to supersonic speeds by solid propellant rocket motors of 20,000-pounds-seconds total impulse and 3-second burning time. Two such rockets mounted in parallel and ignited simultaneously were employed in boosting models 1 and 2. Model 3 was boosted by a single rocket. Photographs of two model and booster combinations on their launchers are presented in figure 4.

The control surfaces were deflected in a continuous square wave by a hydraulic pulsing system. The control deflections utilized were ±8°. Model 3 was equipped with six NACA pulse rockets having total impulses of 6.0 pound-seconds and average durations of 0.08 second. These rockets were mounted in the model so as to provide pitch disturbances.

The physical characteristics of the three models are presented in the following table:

	Model 1	Model 2	Model 3
Weight, lb	122.1	110.4	106.9
I_y, slug - ft^2	15.04	18.35	13.11
Center of gravity, percent $\bar{c}$ ahead of leading edge of $\bar{c}$	63.5	70.3	11.6

Wing:

S_w, sq ft	2.84
$\bar{c}$, ft	1.46
t/c at wing-body juncture	0.03

Canard control surfaces:

S_e, sq ft	0.108
$\bar{c}_e$, in.	3.46
t/c at root chord	0.03

The reference wing area is the total wing area in one plane obtained by extending the wing leading and trailing edges to the body center line.

INSTRUMENTATION

The models were equipped with NACA six-channel telemeters which transmitted normal and longitudinal accelerations, angle of attack, control deflection, total pressure, and a calibrated static pressure. Angle of attack was measured by a free-floating vane mounted on a sting and attached to the nose of the body as reported in reference 2. Total pressure was measured by a total-pressure tube extended below the fuselage, as shown in figure 1.

The model trajectories were determined by an SCR 584 type radar tracking unit and the model velocities by a CW Doppler velocimeter. Radiosondes released at the time of the flights measured temperatures and atmospheric pressures through the altitude range traversed by the models.

TECHNIQUE

After the separation of the model and booster, programmed disturbances were provided by the deflection of control surfaces or the firing of pulse rockets. The resulting oscillations were analyzed by the methods of reference 1 to obtain the stability and control derivatives. The angle of attack measured by the indicator was corrected to the angle at the center of gravity by the methods of reference 3.

ACCURACY

The measured quantities are believed to be accurate within the following limits:

[redacted]

M	Limit of Accuracy				
	M	α	δ	C_L	$C_{D_{min}}$
0.8	±0.02	±0.5	±0.3	±0.030	±0.011
1.3	±.01	±.5	±.3	±.012	±.004
1.8	±.02	±.5	±.3	±.005	±.002

These errors, dependent upon telemeter and radar precision, are primarily systematic in nature; parameters dependent upon differences or slopes of measured quantities, such as C_{L_α} and α/δ, are more accurately determined than the above errors indicate. Other derivatives, C_{L_δ} and $C_{m_q} + C_{m_{\dot{\alpha}}}$, which are determined from mathematical relations involving combinations of measured quantities are of questionable accuracy.

RESULTS AND DISCUSSION

Results are presented from the flights of model 1 (in-line canard configuration), model 2 (interdigitated canard configuration), and model 3 (body-wing configuration). Stability data were obtained from all models; however, control-effectiveness data were only available for model 1.

The scale of the flight tests is presented in figure 5. Reynolds number, based on the wing mean aerodynamic chord, varied from 5.3×10^6 at $M = 0.7$, to 20.5×10^6 at $M = 2.07$.

Sample time histories at supersonic and subsonic speeds from the flight of model 1 are presented in figure 6. The programmed control deflection and the resulting missile response as measured by the angle-of-attack indicator and the normal accelerometer are presented. Also shown are the Mach number variation with time and the magnitude of the longitudinal deceleration.

Static Stability

Periods of oscillation of the models, a measure of static stability, are presented in figure 7. The natural frequencies of the models were nearly the same, varying from $2\frac{1}{2}$ cycles per second at low Mach numbers to nearly 7 cycles per second at a Mach number of 1.90. From the measured periods the static stability derivative C_{m_α} was calculated and is presented in figure 8. The C_{m_α} of models 2 and 3 were corrected to the center-of-gravity location of model 1 for comparison. The C_{m_α} of model 3 (no control surfaces) is about 25 percent greater than that of model 1 (control surface in-line with wing). Also shown for comparison is the C_{m_α} of a similar wing-body configuration tested at a Mach number of 1.62 in the Langley 9-inch supersonic tunnel. The agreement of this data with that of model 3 is good.

The measured lift-curve slopes of models 1 and 2 are presented in figure 9. The lift-curve slope of model 3 was not determined because of normal accelerometer failure. The lift-curve slope varied gradually with Mach number, a peak value of 0.054 occurring at a Mach number of 1.04 and a minimum of 0.0365 at a Mach number of 1.82. From the data available at $M = 2.08$, it appears that interdigitation has no large effect on lift-curve slope.

From the curves of C_{m_α} and C_{L_α}, the aerodynamic-center location was determined and presented in figure 10. At transonic speeds the aerodynamic center shifted rearward approximately 13 percent of $\bar{c}$. Through the supersonic Mach number range, the aerodynamic center varied between 0- and 2-percent $\bar{c}$ back of the leading edge of $\bar{c}$. The data from model 2 at $M = 2.08$ indicate that interdigitation has no large effect on aerodynamic-center location.

Dynamic Stability

The exponential damping constant b is determined from the envelope of the model oscillation and is presented in figure 11. The value of b for the in-line model increased from a minimum of 2.15 at $M = 0.8$ to a maximum of 5.0 at $M = 1.85$. These values of damping correspond to $T_{1/2}$ of 0.32 second and 0.14 second, respectively. The wing-body model had a higher damping exponent because of a smaller moment of inertia.

The total aerodynamic-damping derivative $C_{m_q} + C_{m_{\dot{\alpha}}}$ obtained from the damping exponent by removing the contribution of C_{L_α} according to

the method of reference 1 is presented in figure 12. In the transonic range $C_{m_q} + C_{m_{\dot{\alpha}}}$ decreased to a minimum of -12.3 at $M = 1.03$, followed by an increase to -16.7 at $M = 1.26$. Above $M = 1.26$, $C_{m_q} + C_{m_{\dot{\alpha}}}$ decreased gradually. The damping derivative of model 2 was -19.0 at $M = 2.08$. This apparent increase in $C_{m_q} + C_{m_{\dot{\alpha}}}$ over that of model 1 may be attributed to center-of-gravity shift, interdigitation, unusual variation with Mach number, and, or accuracy of the measurement.

Control Effectiveness

The control derivatives C_{L_δ} and C_{m_δ} of the in-line model are presented in figures 13 and 14. The lift due to canard deflection C_{L_δ} is small at all Mach numbers and shows a negative trend at supersonic speeds. Pitching effectiveness C_{m_δ} increases with Mach number to 0.008 at $M = 1.0$ and decreases through the supersonic region to 0.0065 at $M = 1.80$. The negative C_{L_δ} results from the effect of downwash due to control deflection $\frac{d\epsilon}{d\delta}$. Although $\frac{d\epsilon}{d\delta}$ reduced the total lift, it had favorable effects on pitching effectiveness.

The variation of the trim angle of attack with Mach number is presented in figure 15 for the two nearly equal control deflections. Although it was expected that a symmetrical model would trim at $\alpha = 0$ for $\delta = 0$, the data indicate a varying α_{trim} with Mach number for $\delta = 0$. This apparent out-of-trim may have resulted from an indicator out-of-trim or asymmetries due to model construction.

The test α_{trim} per unit control deflection of the in-line model is presented in figure 16. The test α/δ remains nearly constant through the Mach number range, being 0.23 at $M = 0.74$ and 0.29 at $M = 1.80$.

The steady-state values of $\frac{\Delta a_n/g}{\Delta \delta}$ obtained from the flight test of model 1 were reduced and presented as curves at sea level and 20,000 feet in figure 17. At sea level the values of $\frac{\Delta a_n/g}{\Delta \delta}$ increase gradually from 0.28 at $M = 0.80$ to 0.94 at $M = 1.8$.

For the large static margin of the test (60 percent $\bar{c}$ at supersonic speeds), the effectiveness of the canards in producing angle of attack and normal acceleration was small. If greater maneuverability is desired, however, it is possible to reduce the static margin as much as $0.45\bar{c}$ and still retain a stable configuration at subsonic speeds.

Frequency Response

In the analysis of systems comprised of an airframe and automatic controls, frequency-response methods are employed. The designer, in most instances, must rely on airframe frequency responses calculated from the equations of motion using theoretical and experimental stability derivatives. Frequency responses, however, may also be determined from experimental transient responses. (Both methods are outlined subsequently.) The airframe frequency response of α/δ, determined from the measured transient response at $M = 1.24$ and calculated using the experimental stability derivatives, is presented in figure 18. The curves show good agreement between the two methods except in the amplitude ratio near the natural frequency and the phase angle at high forcing frequencies. The agreement indicates that the response characteristics of this configuration may be accurately calculated within the angle-of-attack range of the flight test from the equations of motion using experimental stability derivatives.

When the linearized longitudinal equations of motion presented in reference 4, with the exception of the longitudinal force equation, are used, the transfer function is:

$$\frac{\alpha}{\delta}(D) = \frac{CFD - (CF + AH)}{-AED^2 + (AF + AJ - BE)\,D + (AG + BF)}$$

where:

$$A = \frac{mV}{57.3qS_w} \qquad F = \frac{1}{57.3}\,C_{m_q}\bar{c}/2V$$

$$B = C_{L_\alpha} \qquad G = C_{m_\alpha}$$

$$C = C_{L_\delta} \qquad H = C_{m_\delta}$$

$$E = \frac{I_y}{57.3qS_w\bar{c}} \qquad J = \frac{1}{57.3}\,C_{m_{\dot{\alpha}}}\bar{c}/2V$$

$$D = \frac{d}{dt}$$

C_{m_q} was assumed to be $= 0.90\left(C_{m_q} + C_{m_{\dot{\alpha}}}\right)$

When $i\omega$ is substituted for D in the transfer function and complex variable methods are used, the amplitude ratio α/δ and phase angle φ are calculated using the experimental stability derivatives as indicated in reference 4 for any forcing frequencies.

The measured α transient responses may be operated on by the method of reference 5 to determine the actual missile frequency response. The output is represented by a series of step-functions which, along with the square wave input, are transformed into the frequency domain by Fourier series expansions. The missile frequency response is determined from these series by the following equation:

$$\text{Output} = \text{Input} \times \text{transfer function}$$

In performing the calculations the resultant complex exponential series was summed with the aid of an electromechanical synthesizer to obtain the real and imaginary vectors. This operation is more fully explained in reference 6.

Drag

Drag was determined from the measured angles of attack and longitudinal and normal accelerations and analyzed for $C_{D_{min}}$, $(L/D)_{max}$, and $dC_D/dC_L{}^2$.

The maximum lift-drag ratios are presented in figure 19. Lift-drag ratio remained nearly constant at supersonic velocities, being a maximum of 3.3 at a Mach number of 1.3 and a minimum of 3.1 at Mach numbers of 1.80 and 1.05. Below a Mach number of 1, the ratio L/D increased gradually to a value of 3.85 at a Mach number of 0.80. The data of model 2 at a Mach number of 2.08 indicated the same L/D. The variation of minimum drag coefficient with Mach number is presented for models 1 and 3 in figure 20. The minimum drag coefficient of model 1 with an 8° control deflection increases through the high subsonic Mach numbers from 0.038 at $M = 0.8$ to 0.07 at $M = 1.03$. With increasing Mach number $C_{D_{min}}$ decreased gradually to 0.0435 at $M = 1.82$. Removing the canards reduced $C_{D_{min}}$ about 7 percent between $M = 1.30$ and 1.48 as shown by model 3.

In figure 21 is presented the change in C_D with $C_L{}^2$. The curve of $dC_D/dC_L{}^2$ resembles $1/57.3C_{L_\alpha}$ but is seen to be greater throughout the test Mach number range. The drag due to lift decreases from 0.44 at $M = 0.8$ to 0.37 at $M = 1.1$, followed by an increase with increasing Mach number to a maximum value of 0.50 at $M = 1.80$. The $dC_D/dC_L{}^2$ of the interdigitated model is in agreement with that of the in-line model.

Comparison of Two Canard Models Having Different Area Control Surfaces

Results of similar models having an exposed wing-canard area ratio of 9:1 and 16:1 were compared to show the effect of canard area on stability and control characteristics. Models used in this investigation were model of reference 1, model 1 of this paper, and model A of reference 2. The comparison indicated a noticeable effect of canard area on three parameters; pitching effectiveness, aerodynamic-center location, and total hinge moment.

The effect of canard area on pitching effectiveness is shown in figure 22. The reduction of C_{m_δ} throughout the Mach number range is about the same percentage as the reduction in the canard area. The effect of canard area on aerodynamic-center location is shown in figure 23. A reduction in canard area resulted in rearward shift of aerodynamic-center location of 9 to 14 percent $\bar{c}$.

The total hinge moment required to maintain trim flight at 1° angle of attack $\Delta H/\Delta\alpha$ throughout the Mach number range for model 1 and model of reference 1 are presented in figure 24 for sea-level conditions. Since the hinge moment was not measured on model 1, C_{h_α} and C_{h_δ} for the small canards from reference 2 were combined with α/δ of model 1 to obtain $\Delta H/\Delta\alpha$ by the relation $\Delta H/\Delta\alpha = H_\alpha + (\delta/\alpha)H_\delta$. By the use of C_{h_α}, C_{h_δ}, and α/δ of the model of reference 1, the relation $\Delta H/\Delta\alpha$ for the large canard model was similarily obtained for the same static stability of model 1. The hinge moment required for trim flight was small for both controls at supersonic speeds, whereas the large canards exhibited nearly twice the hinge moments of the small canards at transonic speeds.

CONCLUSIONS

Three cruciform missile configurations, an in-line canard configuration having an exposed wing-canard area ratio of 16:1, an interdigitated canard configuration with the same wing-canard area ratio, and a wing-body configuration without canards, were flight-tested at Mach numbers of 0.75 to 1.80, a Mach number of 2.08, and Mach numbers of 1.25 to 1.45, respectively. Data from these tests indicate the following conclusions:

1. The stability derivatives of the models tested varied gradually with Mach number with the exception of the damping-in-pitch derivative. The damping-in-pitch derivative for the in-line canard configuration was

a minimum at a Mach number of 1.03, increased to a peak value at a Mach number of 1.26, and decreased gradually to a Mach number of 1.82. The lift-curve slope of the in-line canard configuration was a maximum of 0.0540 at a Mach number of 1.04 and a minimum of 0.0365 at a Mach number of 1.82. The aerodynamic-center location of the in-line canard configuration shifted rearward 13 percent of the mean aerodynamic chord at transonic speeds and remained nearly constant at the leading edge of the mean aerodynamic chord for supersonic speeds. The pitching-moment-curve slope C_{m_α} for the model having no canards was 25 percent greater than C_{m_α} of the in-line canard configuration. Available data from the interdigitated configuration indicated no large effect on stability derivatives due to interdigitation.

2. Pitching effectiveness C_{m_δ} of the in-line configuration was maintained throughout the Mach number range. The steady-state angle of attack per unit control deflection $\Delta\alpha/\Delta\delta$ and the normal acceleration per unit control deflection $\frac{\Delta a_n/g}{\Delta\delta}$ were small as the result of a large static margin.

3. The maximum lift-drag ratio of the in-line canard configuration remained nearly constant at supersonic speeds. The minimum drag coefficient of the in-line canard configuration decreased from a maximum value of 0.070 at a Mach number of 1.03 to 0.0435 at a Mach number of 1.82. The effect of removing the canards was noted by the 7-percent reduction of minimum drag coefficient between the in-line canard and the wing-body configurations.

4. The results of the in-line canard configuration were compared with the results of a similar configuration having larger control area (exposed wing-canard area ratio of 9:1). Reducing the canard area decreased the pitching effectiveness proportionally, shifted the aerodynamic-center location rearward 9 to 14 percent of the mean aerodynamic chord, and reduced the total hinge moments required for 1° trimmed flight about 50 percent at transonic speeds.

Langley Aeronautical Laboratory
National Advisory Committee for Aeronautics
Langley Field, Va.

REFERENCES

1. Niewald, Roy J., and Moul, Martin T.: The Longitudinal Stability, Control Effectiveness, and Control Hinge-Moment Characteristics Obtained from a Flight Investigation of a Canard Missile Configuration at Transonic and Supersonic Speeds. NACA RM L50I27, 1950.

2. Brown, Clarence A., Jr., and Lundstrom, Reginald R.: Flight Investigation from Mach Number 0.8 to Mach Number 2.0 To Determine Some Effects of Wing-to-Tail Distance on the Longitudinal Stability and Control Characteristics of a 60° Delta-Wing - Canard Missile. NACA RM L52C26, 1952.

3. Mitchell, Jesse L., and Peck, Robert F.: An NACA Vane-Type Angle-of-Attack Indicator for Use at Subsonic and Supersonic Speeds. NACA RM L9F28a, 1949.

4. Greenberg, Harry: Frequency-Response Method for Determination of Dynamic Stability Characteristics of Airplanes With Automatic Controls. NACA Rep. 882, 1947. (Supersedes NACA TN 1229.)

5. Seamans, Robert C., Jr., Bromberg, Benjamin G., and Payne, L. E.: Application of the Performance Operator to Aircraft Automatic Control. Jour. Aero. Sci., vol. 15, no. 9, Sept. 1948, pp. 535-555.

6. Cornell, Sidney: Instruction Manual for the 24 Unit Fourier Synthesize Developed for the National Advisory Committee for Aeronautics by the Massachusetts Institute of Technology Under N.A.C.A. Contract No. NA_W-5852-Computing Machine. Eng. Memo. No. 6445-E-42, Instrumentation Lab., M.I.T., July 28, 1950.

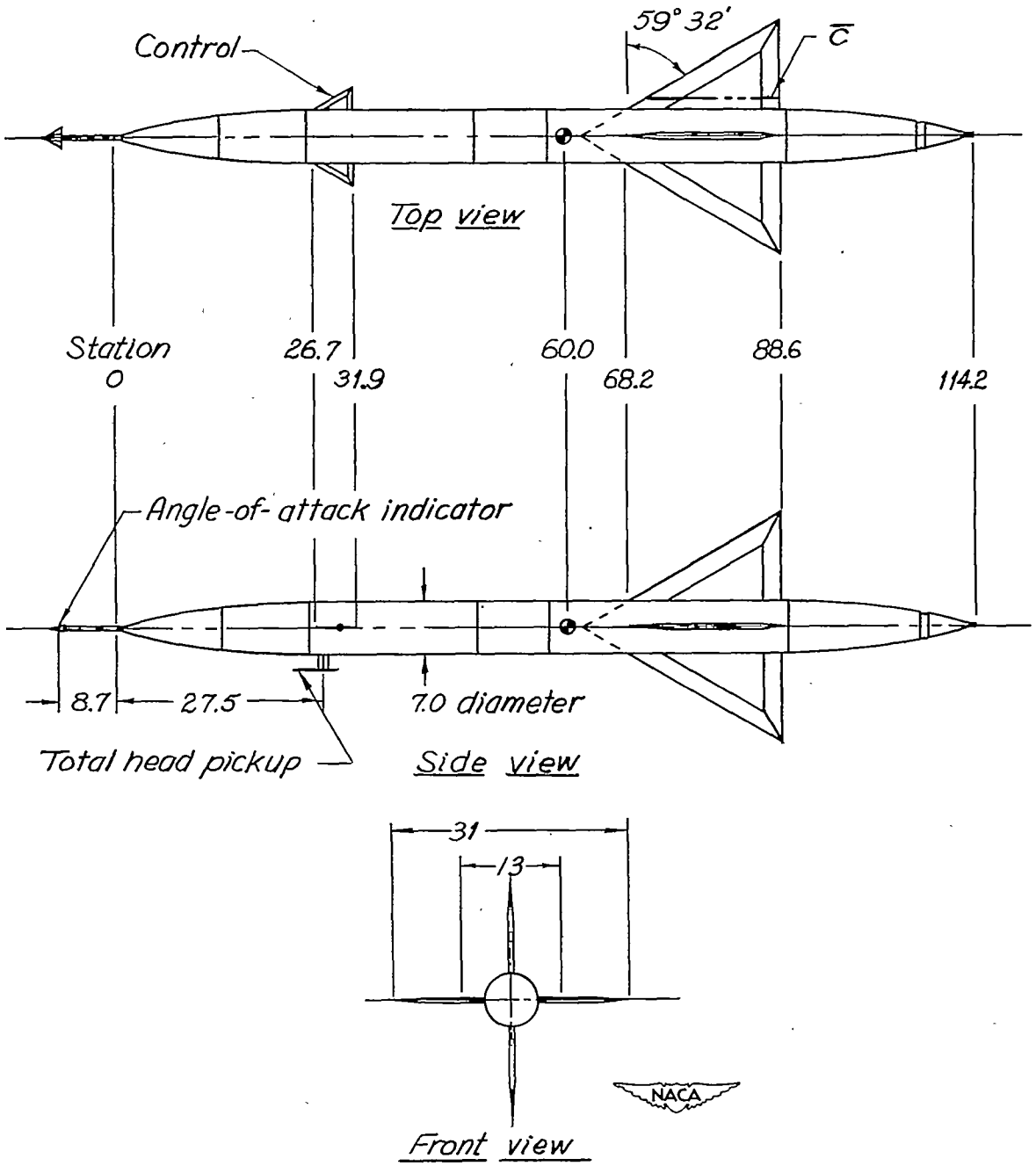

(a) Model 1.

Figure 1.- Model arrangement. All dimensions are in inches.

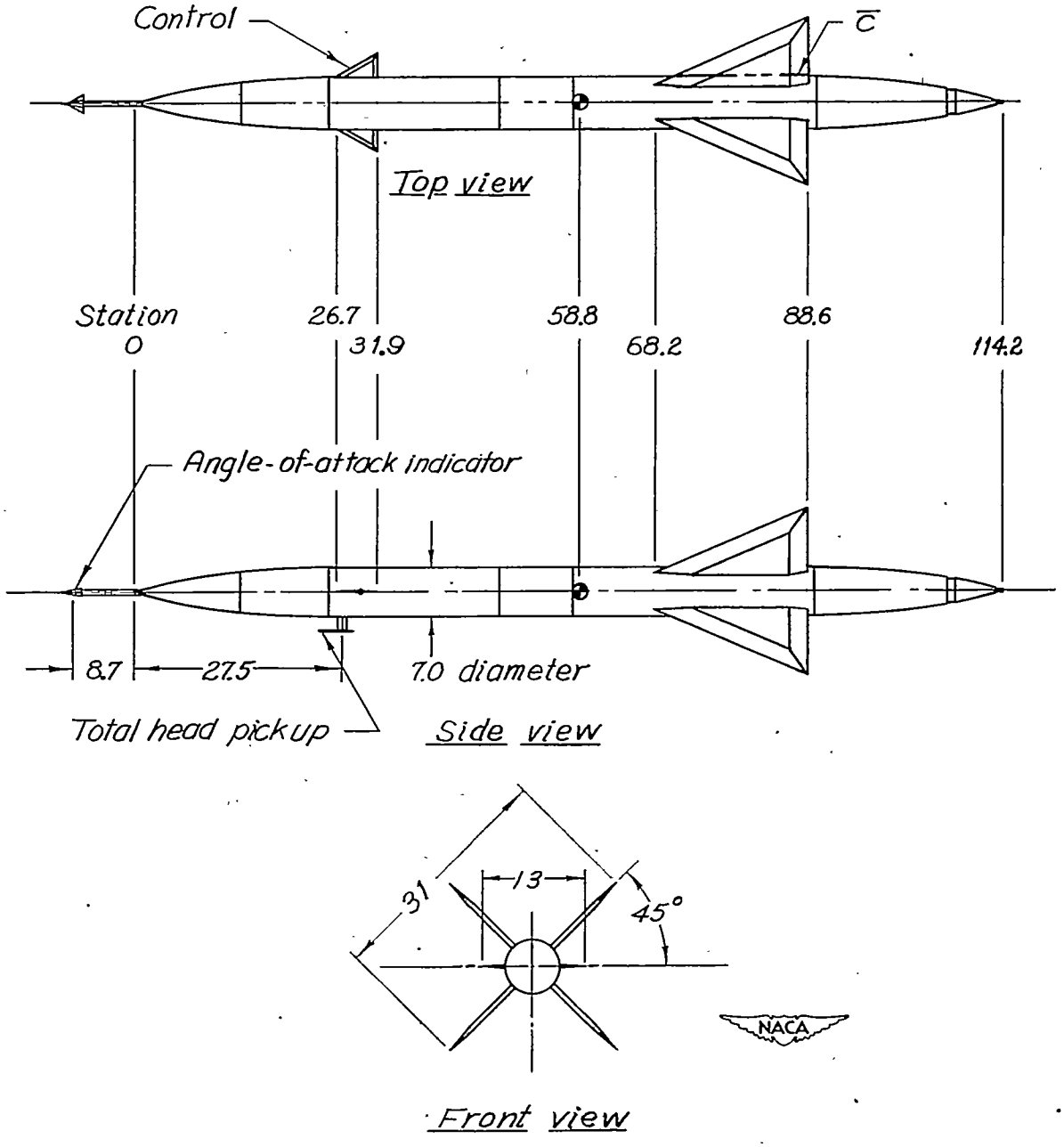

(b) Model 2.

Figure 1.- Continued.

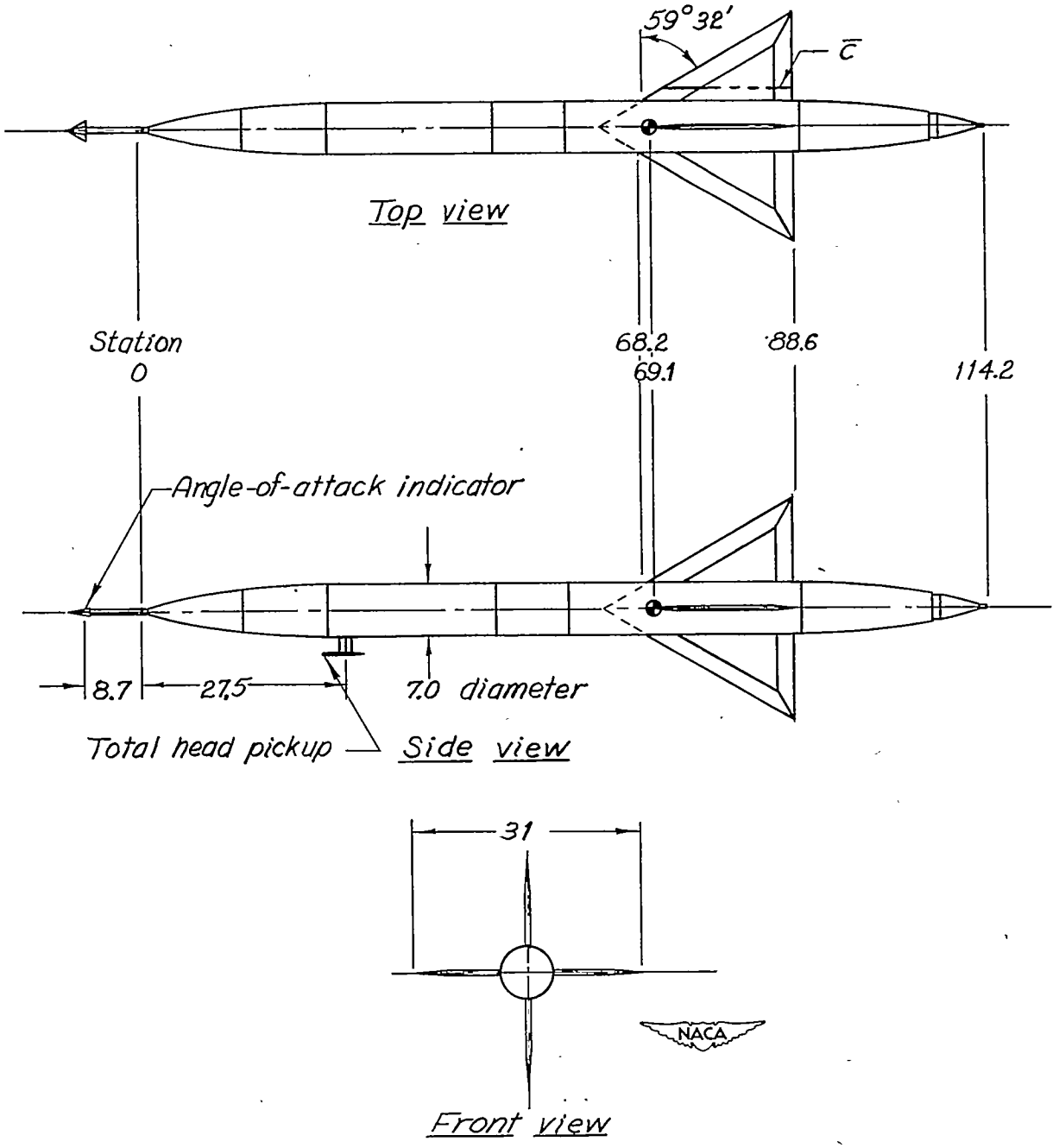

(c) Model 3.

Figure 1.- Concluded.

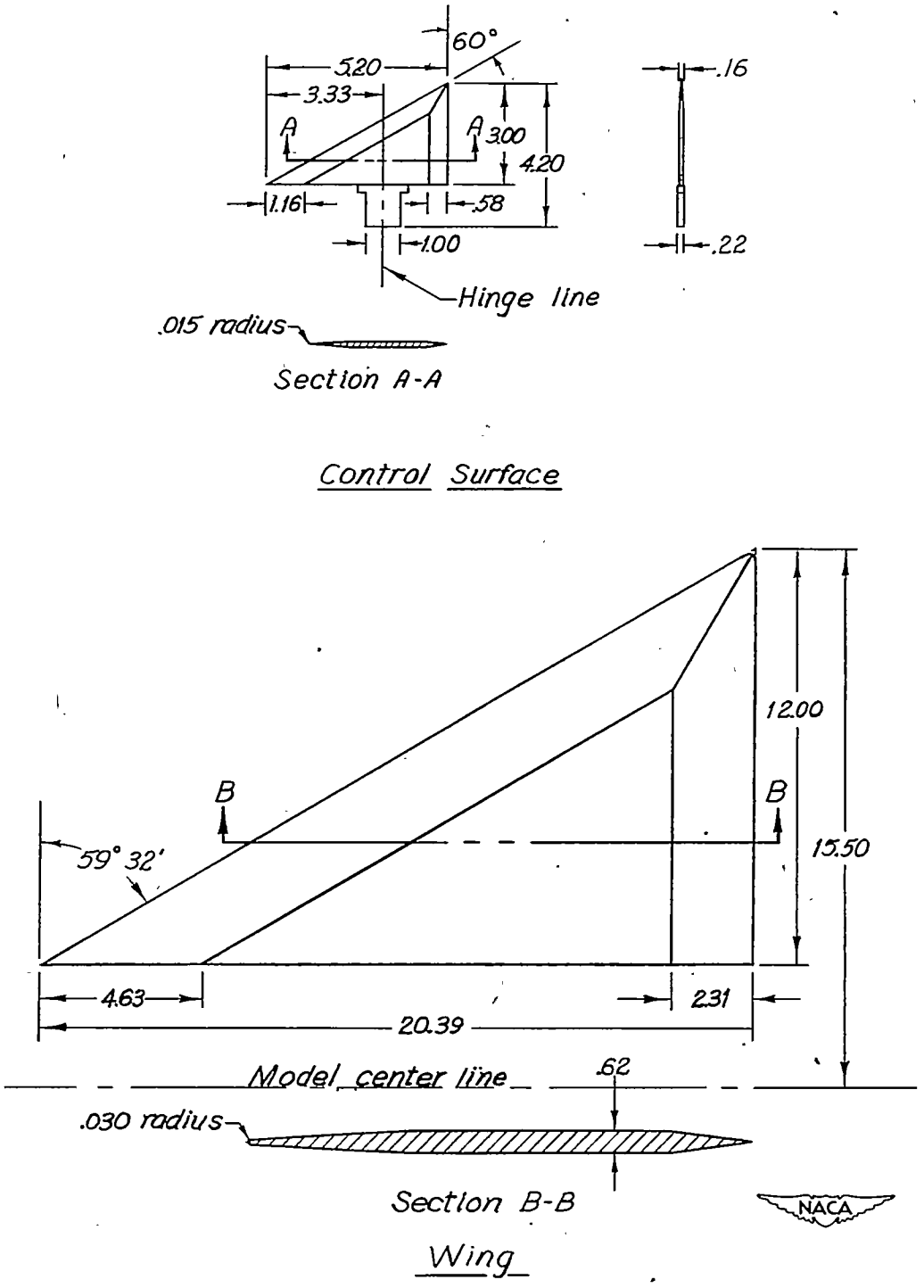

Figure 2.- Wing and control-surface detail. All dimensions are in inches.

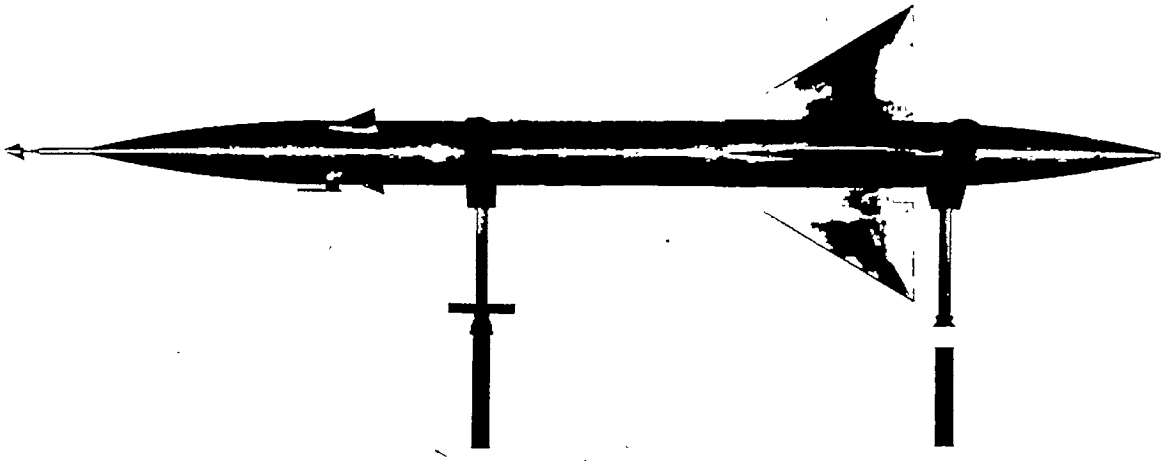

(a) Side view of model. (Model 2)

L-65954

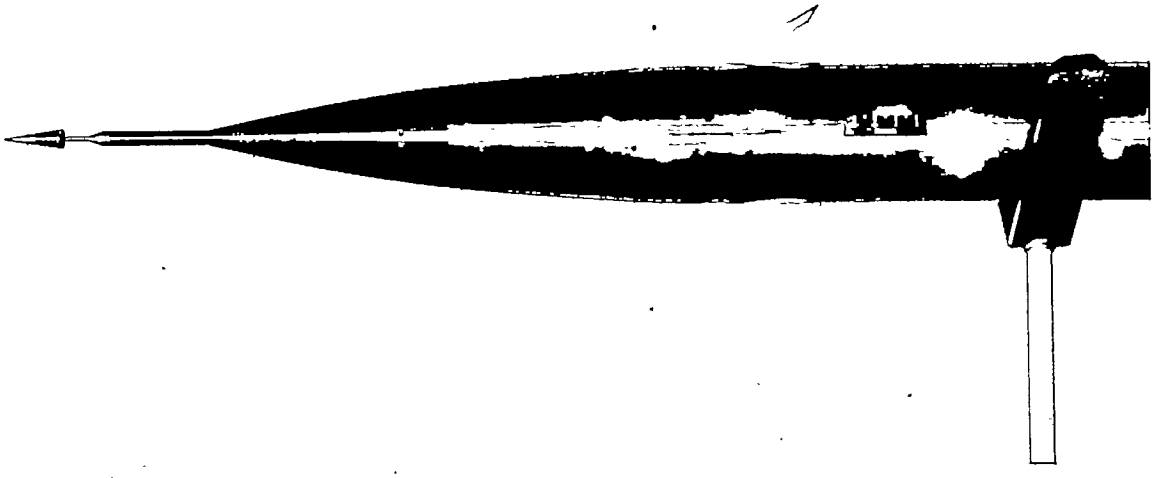

(b) Bottom view showing controls. (Models 1 and 2)

L-65955

Figure 3.- Typical configuration of models tested.

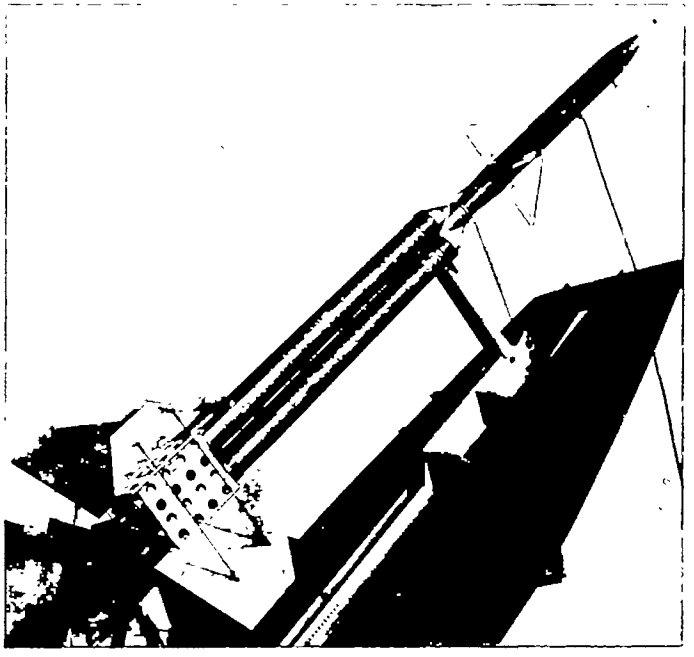

(a) Model 1.

L-63234

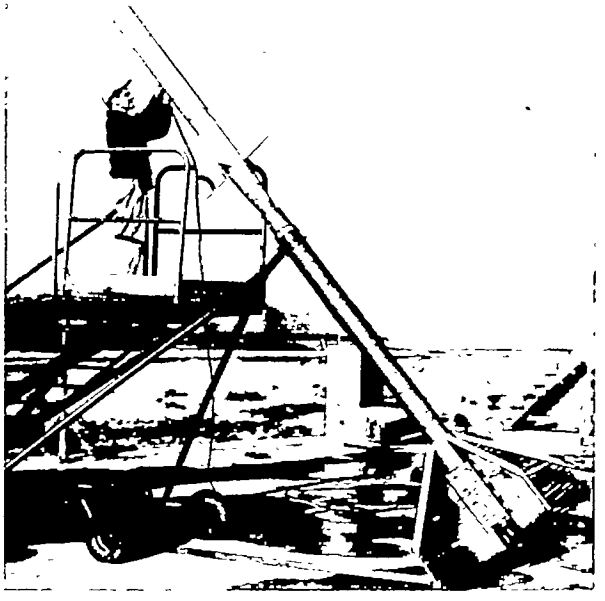

(b) Model 3.

L-63229

Figure 4.- Model-booster combinations at launch.

[redacted]

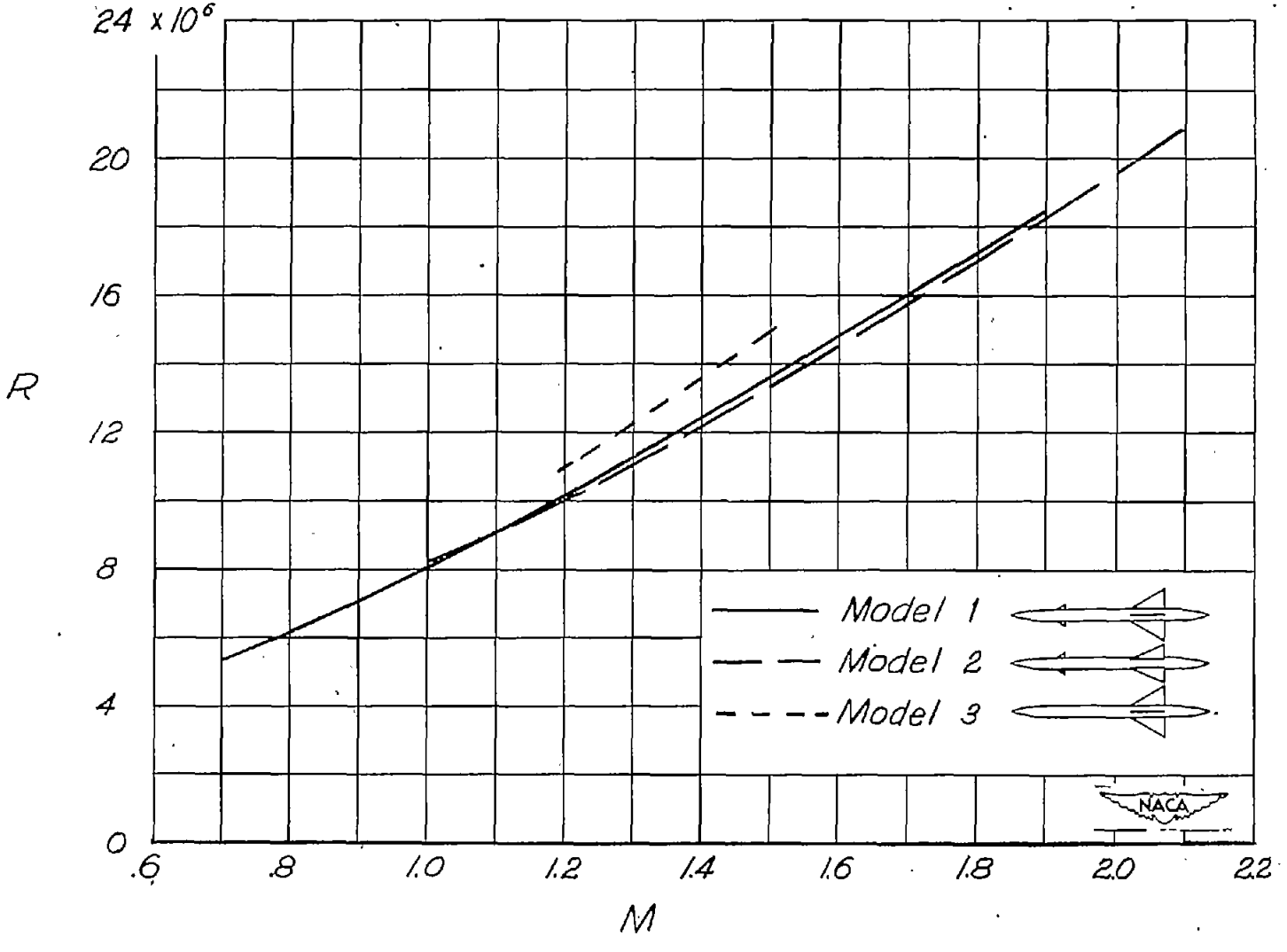

Figure 5.- Variation of Reynolds number with Mach number.

[redacted]

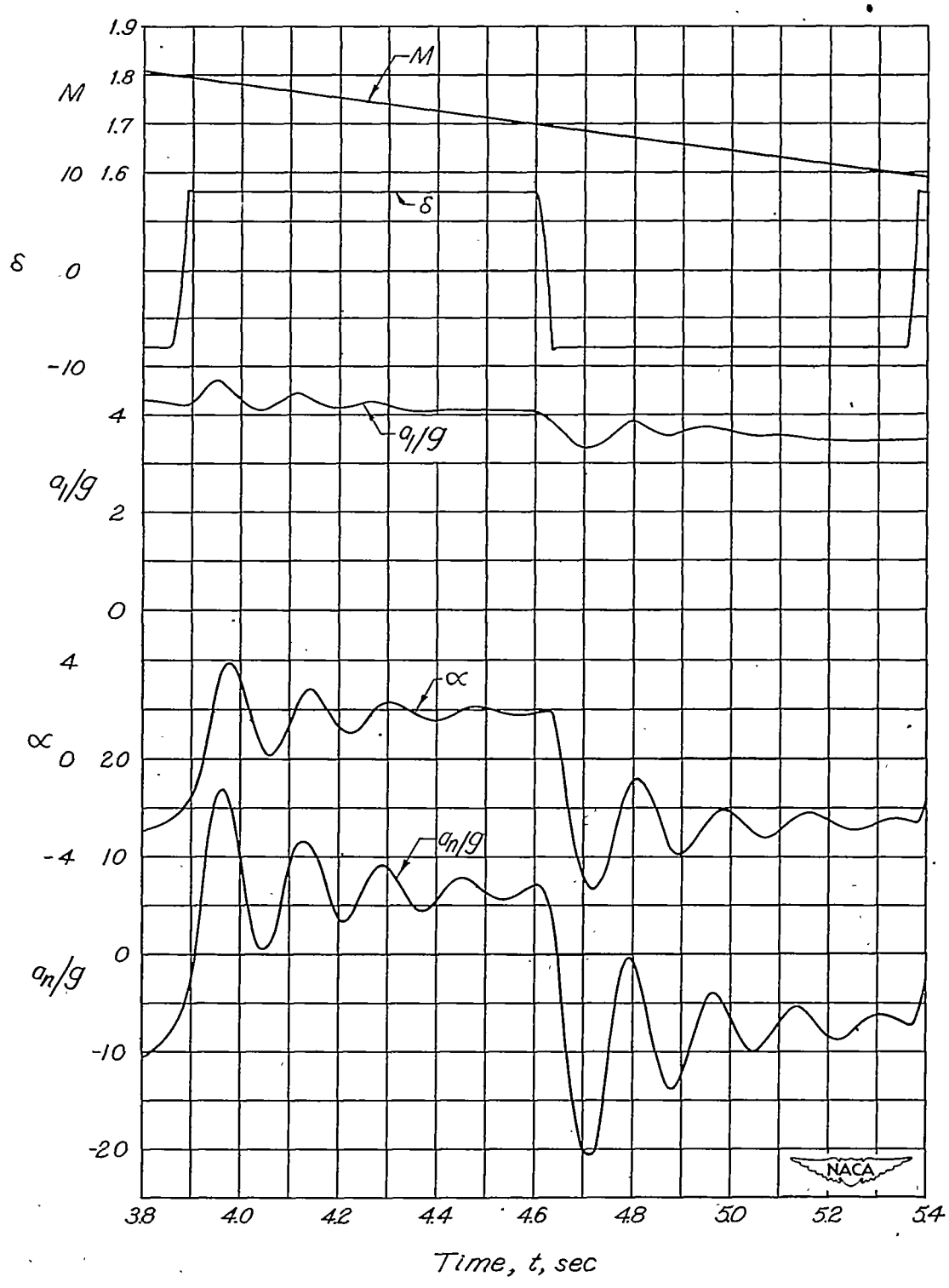

(a) Supersonic.

Figure 6.- Sample time history from the flight of model 1.

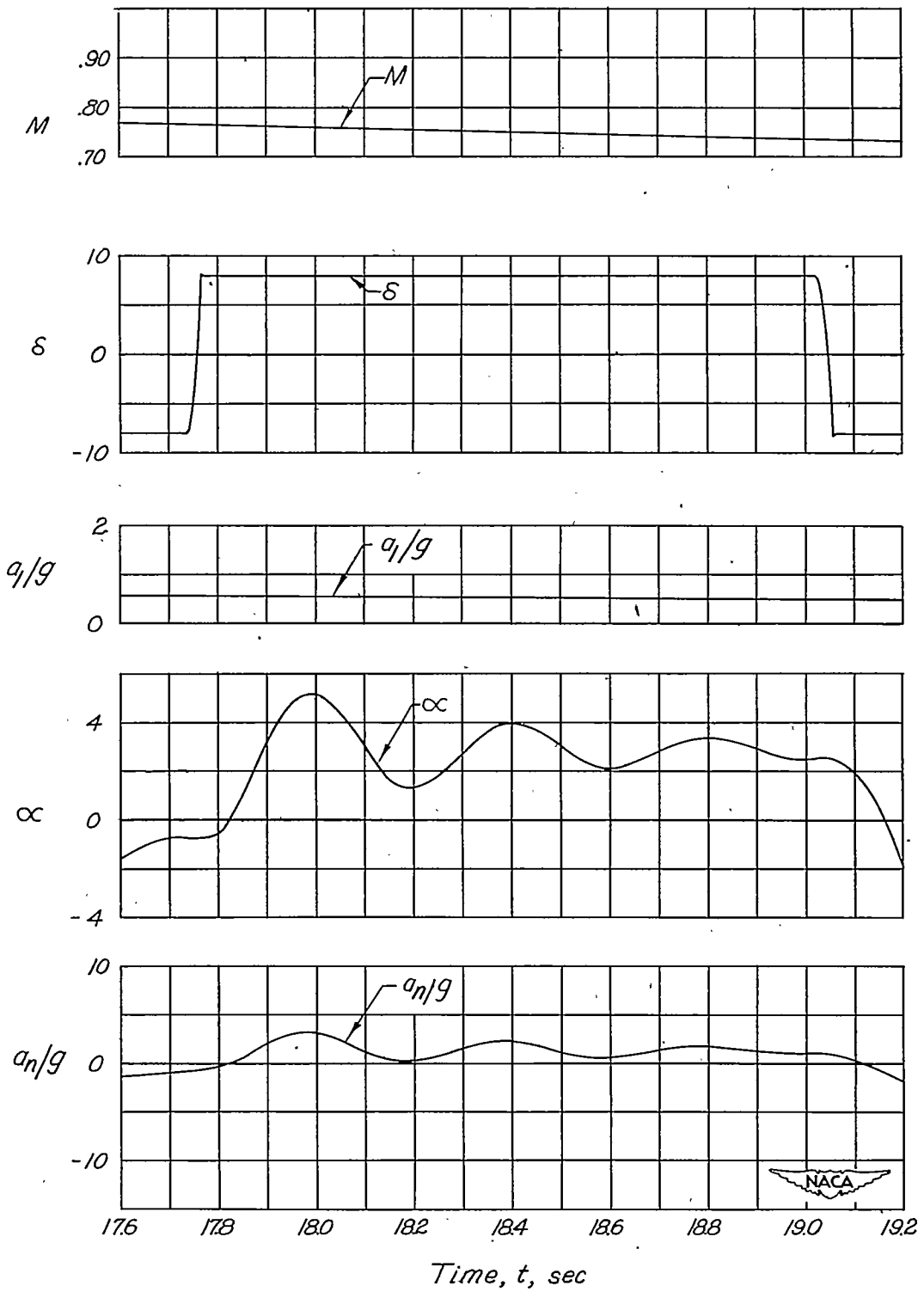

(b) Subsonic.

Figure 6.- Concluded.

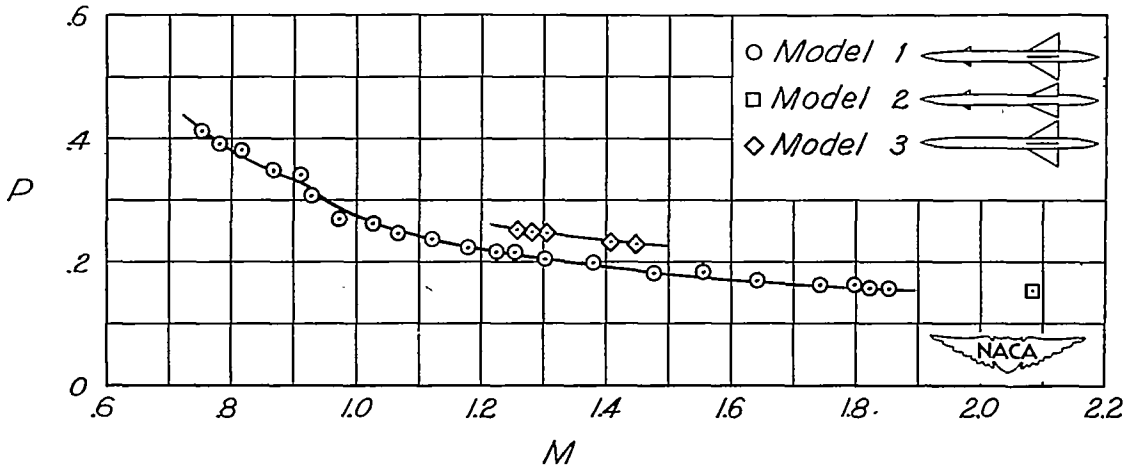

Figure 7.- Variation of period with Mach number.

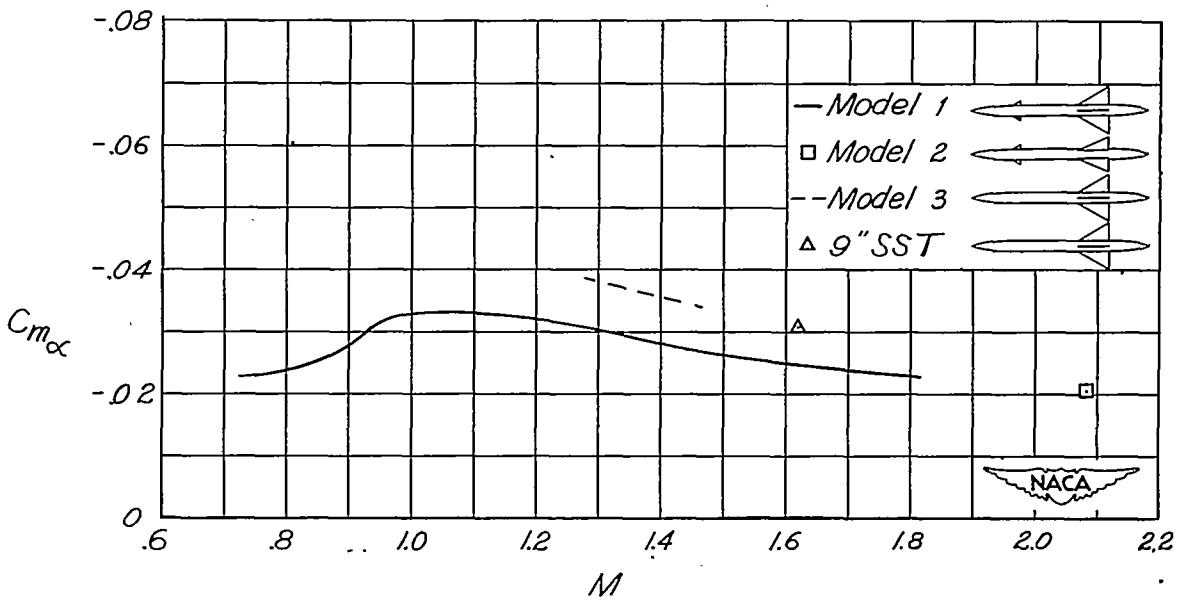

Figure 8.- Variation of static stability derivative with Mach number.

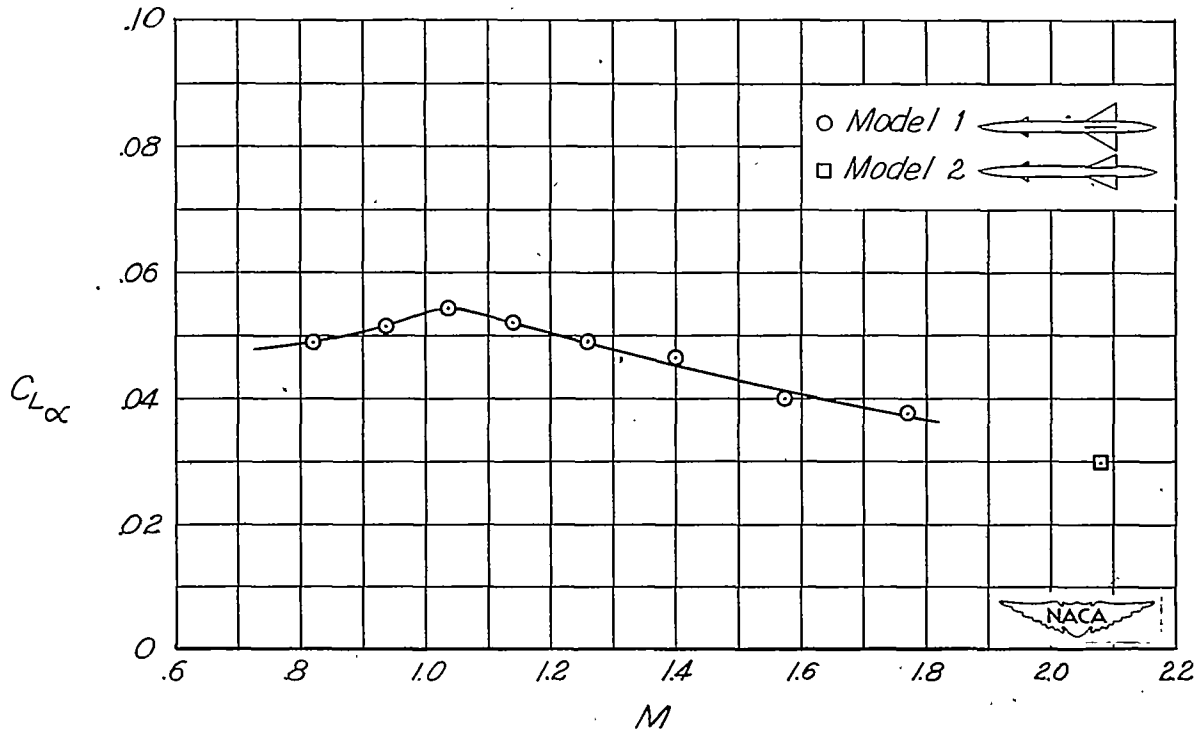

Figure 9.- Variation of lift-curve slope with Mach number.

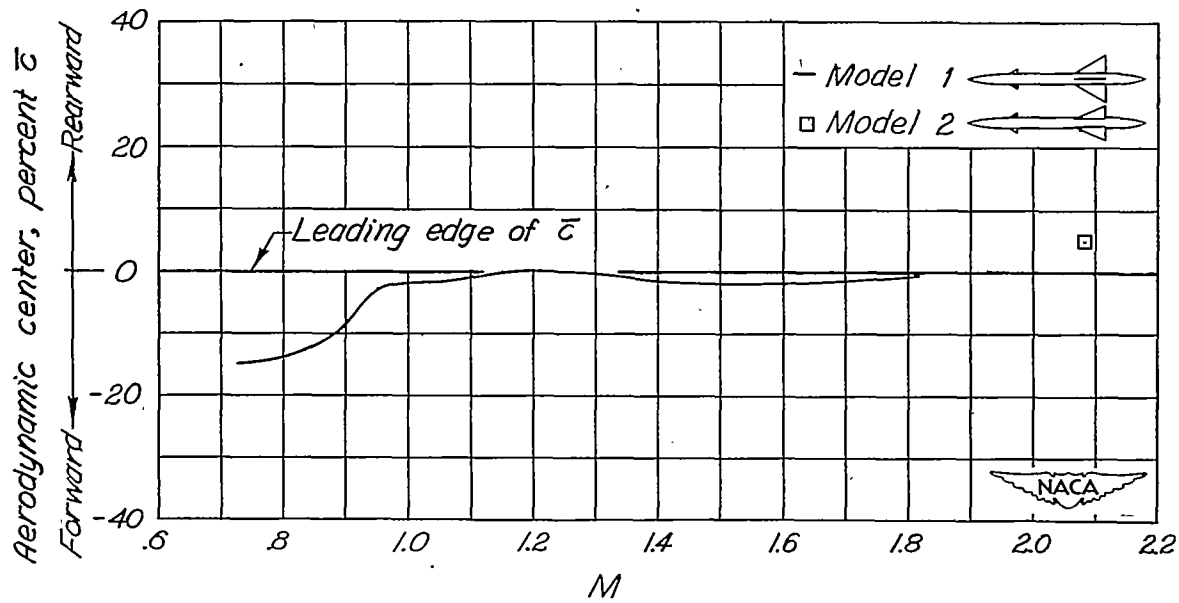

Figure 10.- Variation of aerodynamic-center location with Mach number.

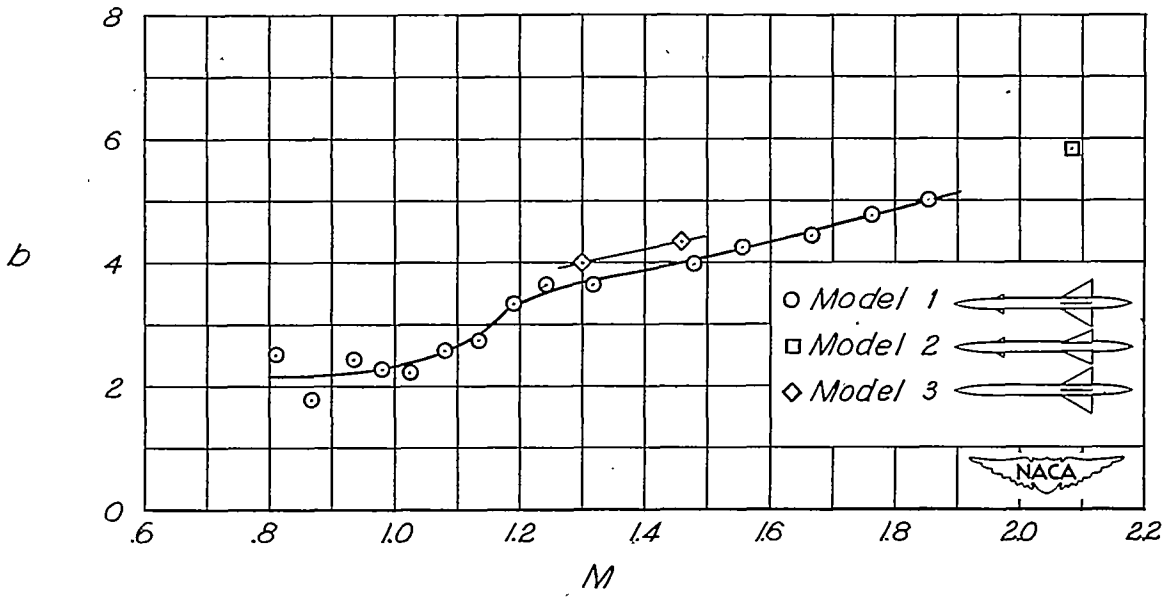

Figure 11.- Variation of exponential damping constant b with Mach number.

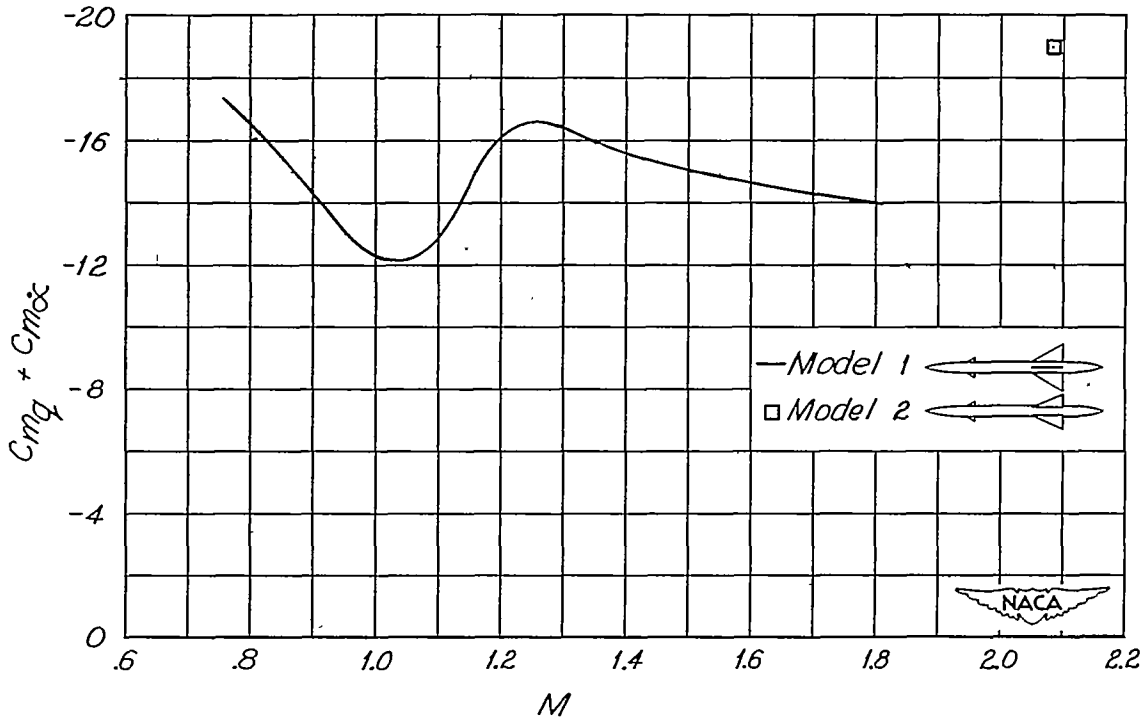

Figure 12.- Variation of aerodynamic damping-in-pitch derivative $C_{m_q} + C_{m_{\dot{\alpha}}}$ with Mach number.

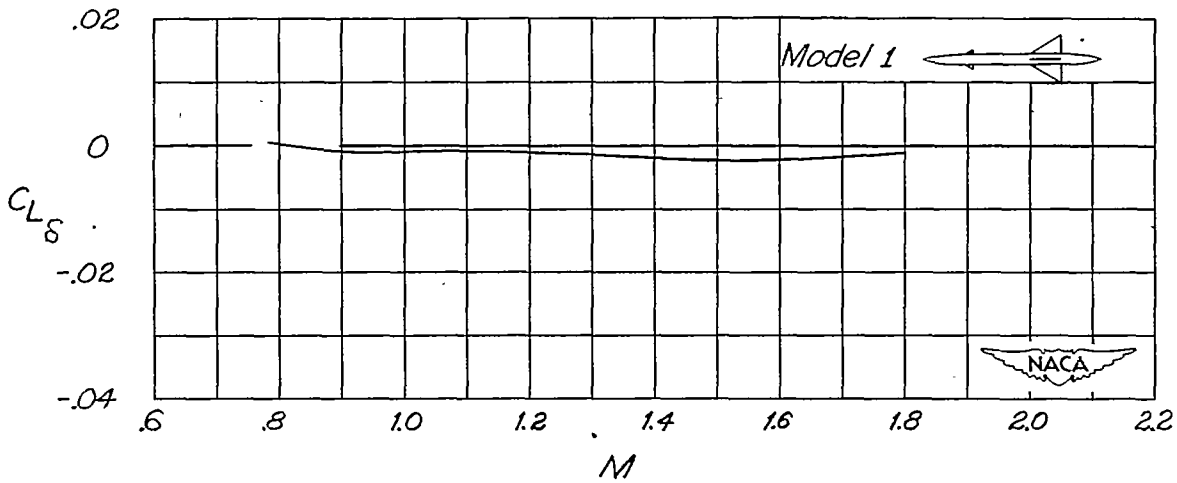

Figure 13.- Effectiveness of control surfaces in producing model lift.

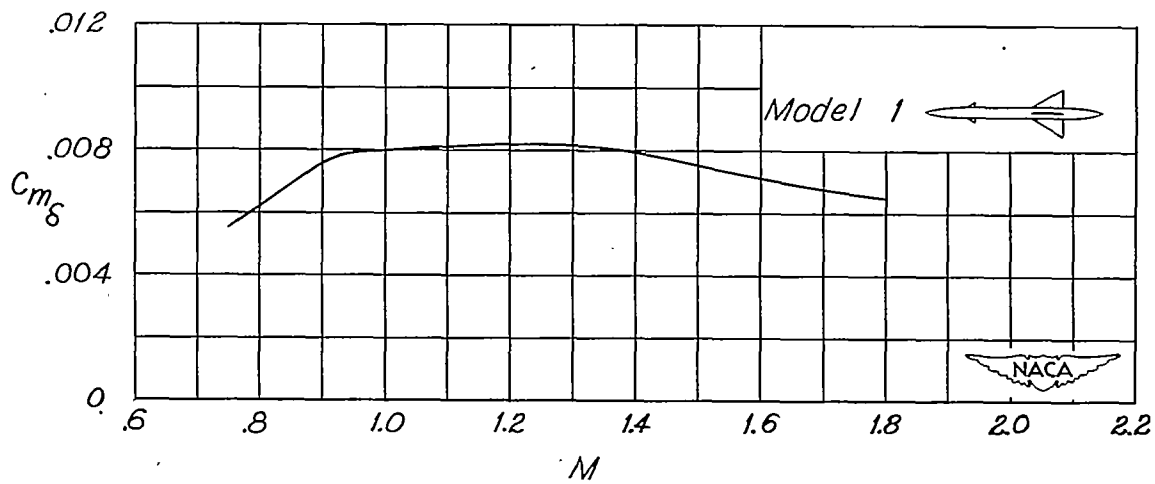

Figure 14.- Effectiveness of control surfaces in producing model pitching moment.

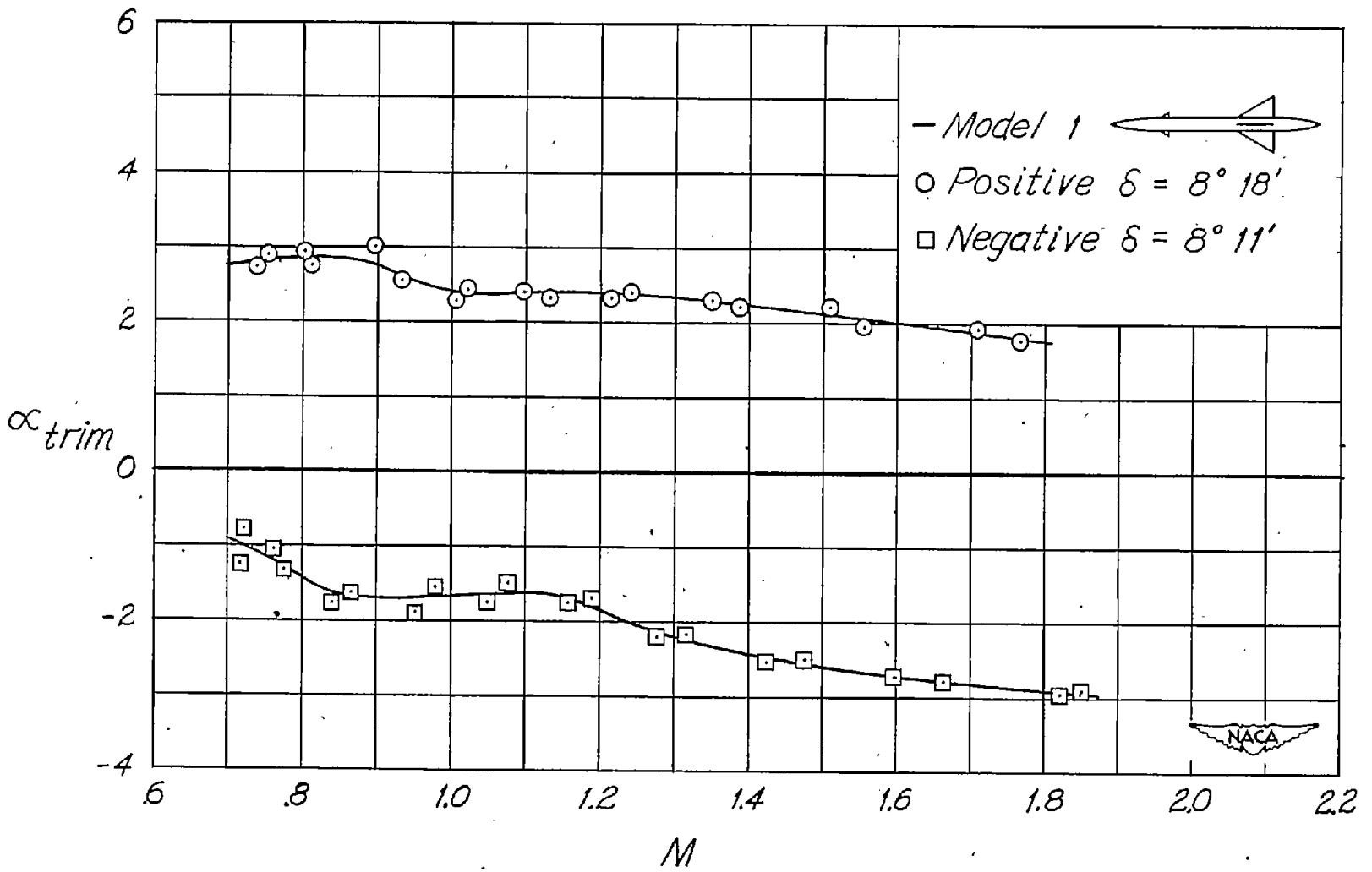

Figure 15.- Variation of trim angle of attack with Mach number.

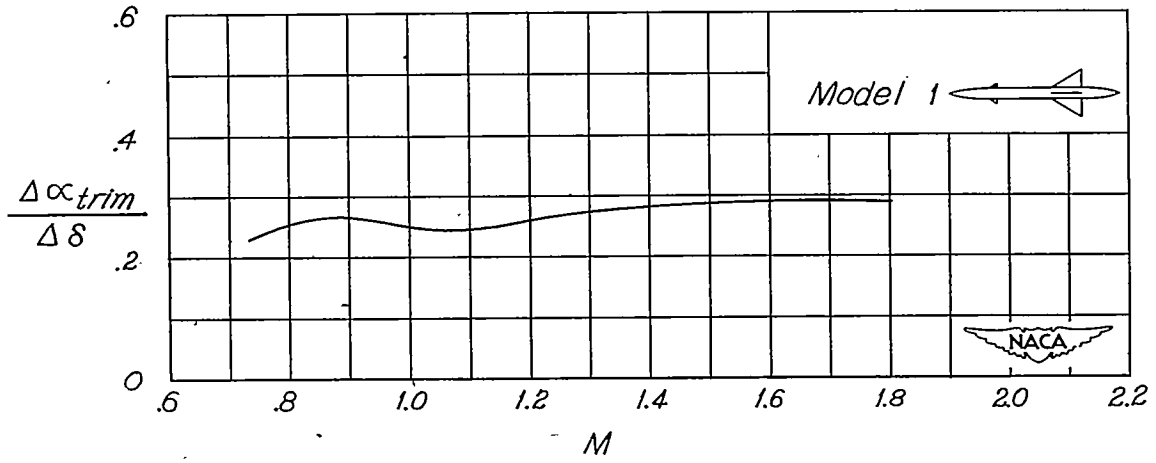

Figure 16.- Trim angle-of-attack produced by a unit control deflection.

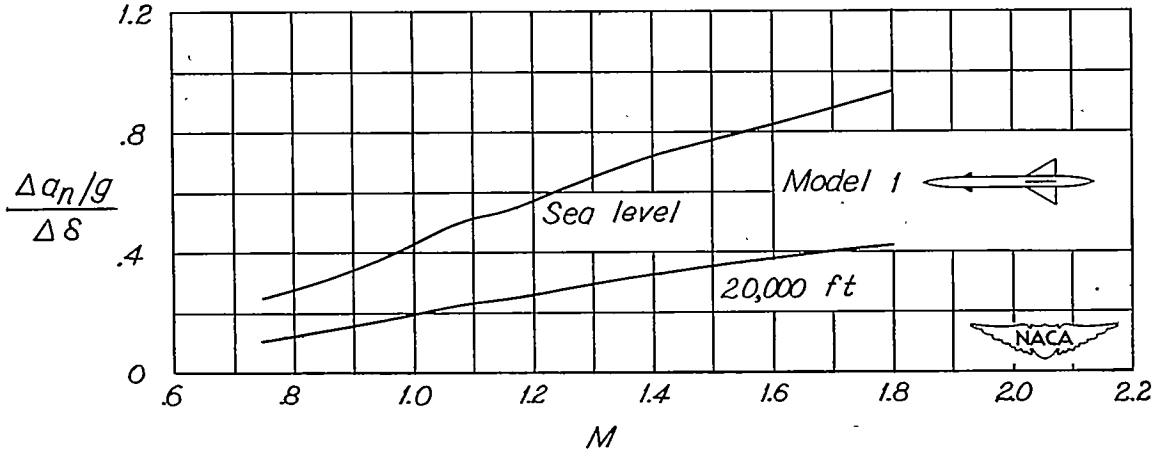

Figure 17.- Trim normal acceleration produced by a unit control deflection.

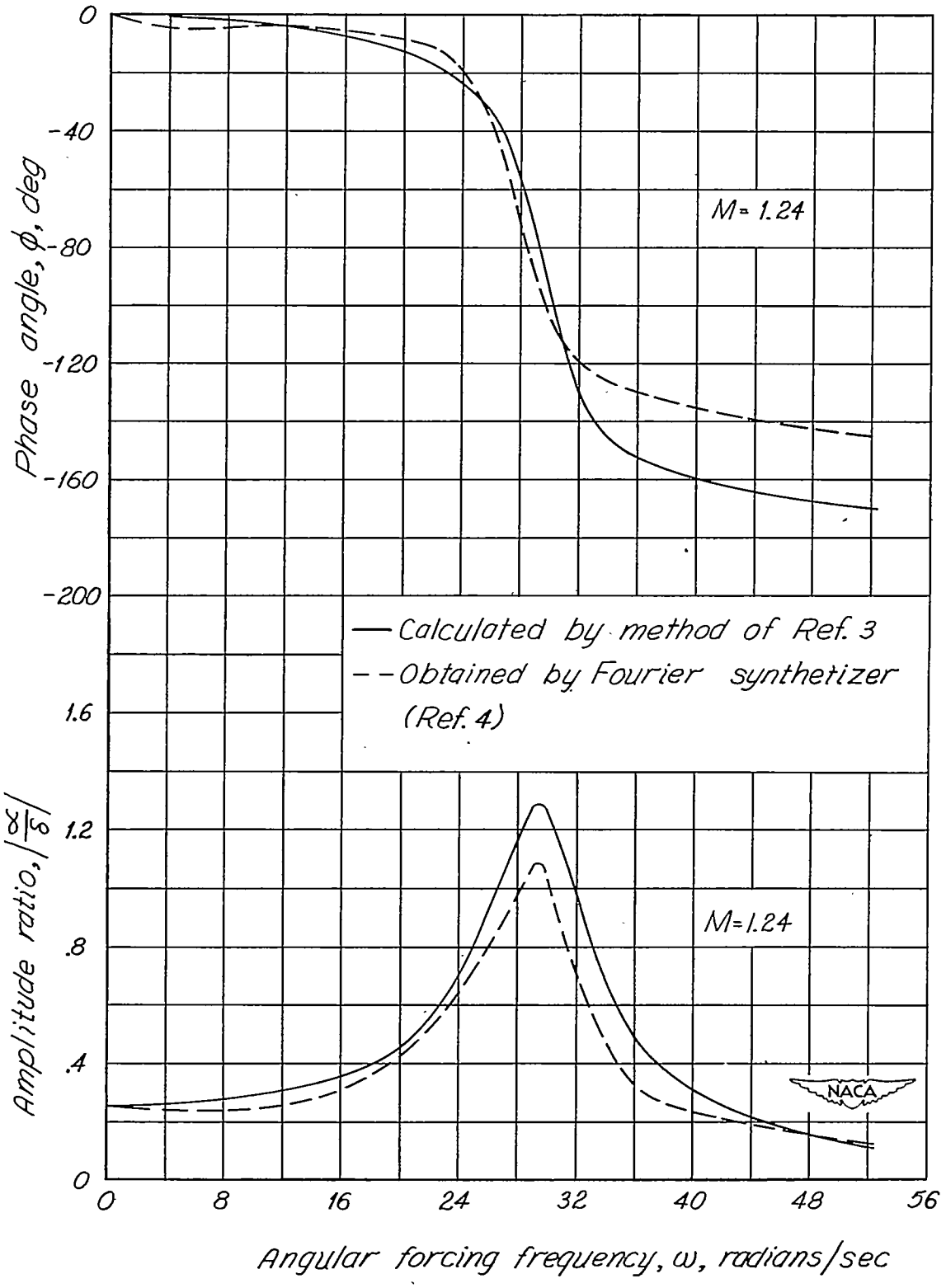

Figure 18.- Angle-of-attack frequency response obtained by two methods from flight-test data of model 1.

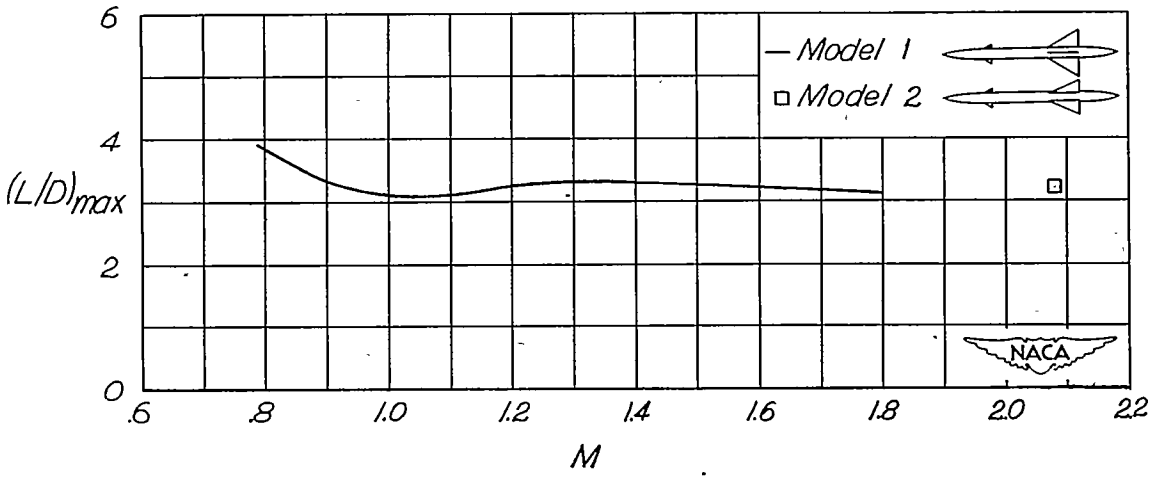

Figure 19.- Maximum lift-drag ratio.

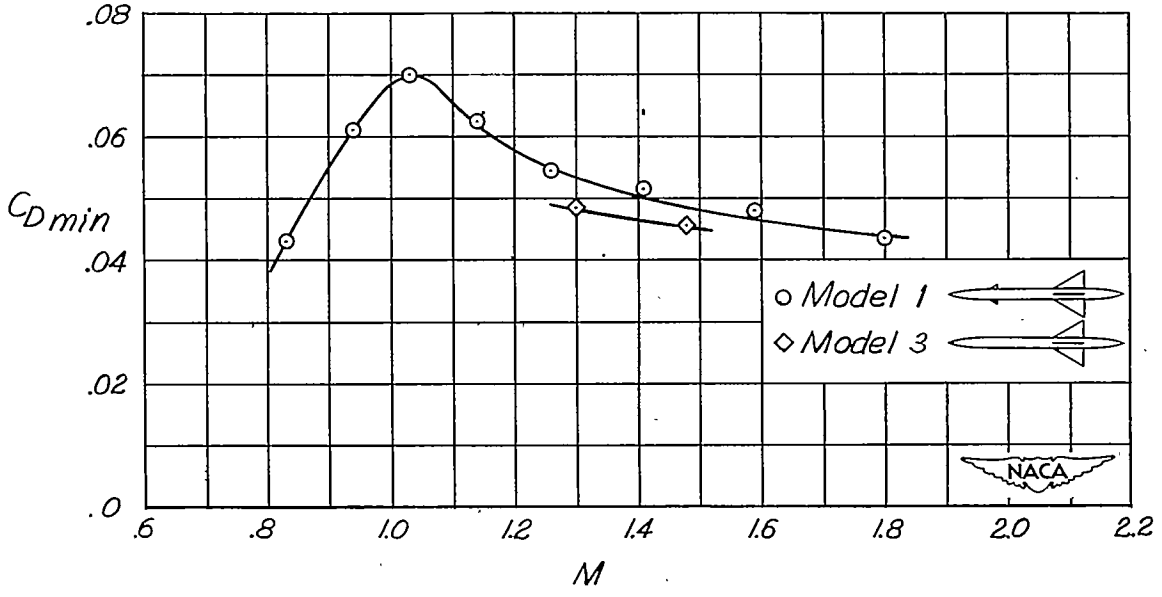

Figure 20.- Minimum drag coefficient.

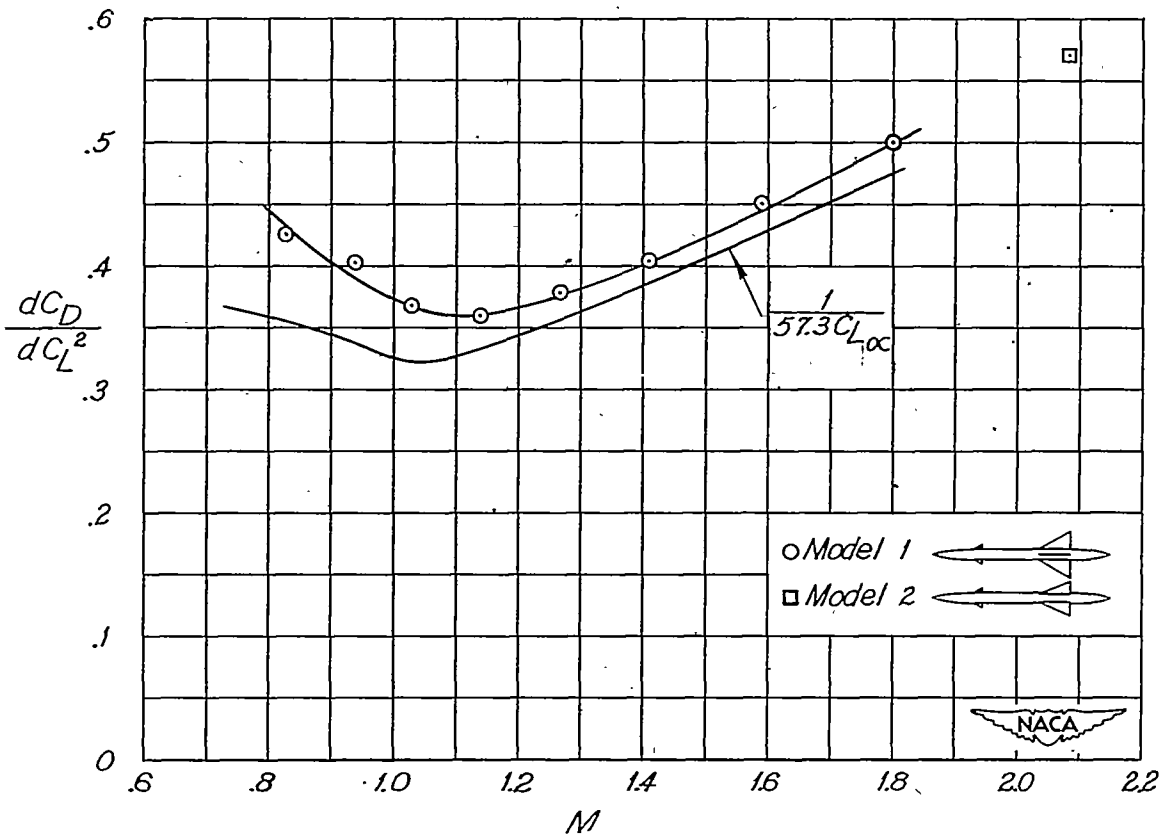

Figure 21.- Effect of lift on drag.

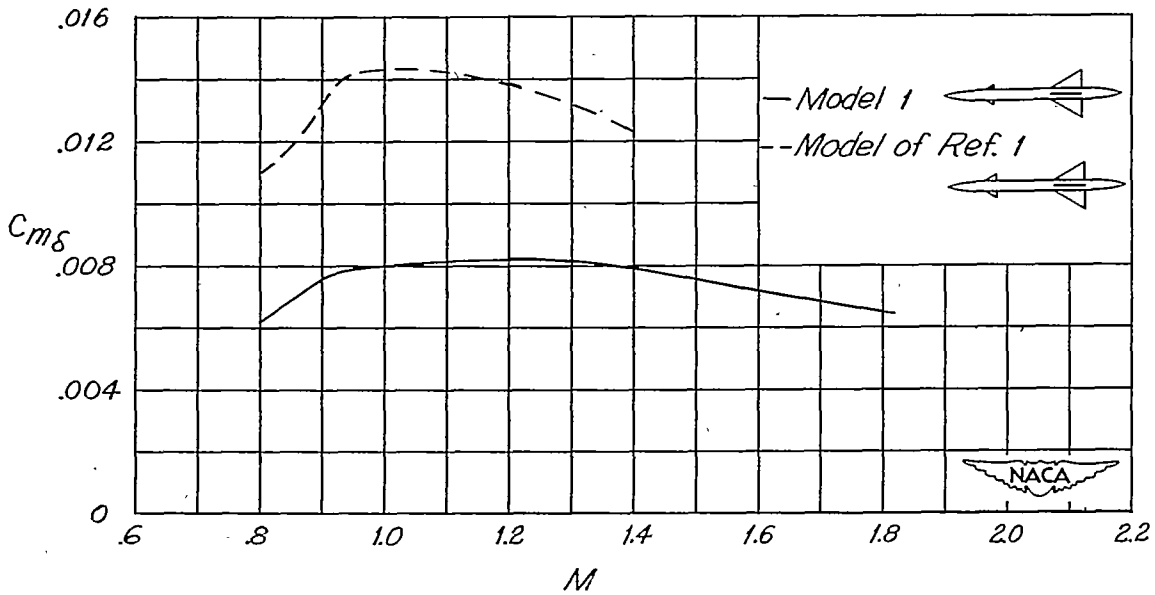

Figure 22.- Effect of control area on pitching effectiveness.

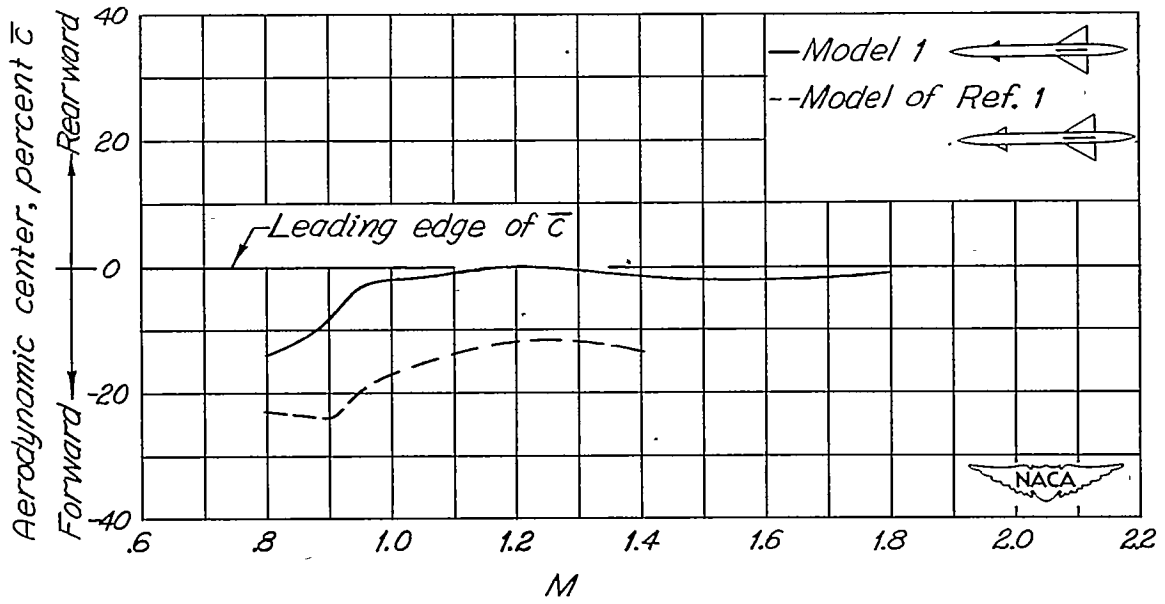

Figure 23.- Effect of canard area on aerodynamic-center location.

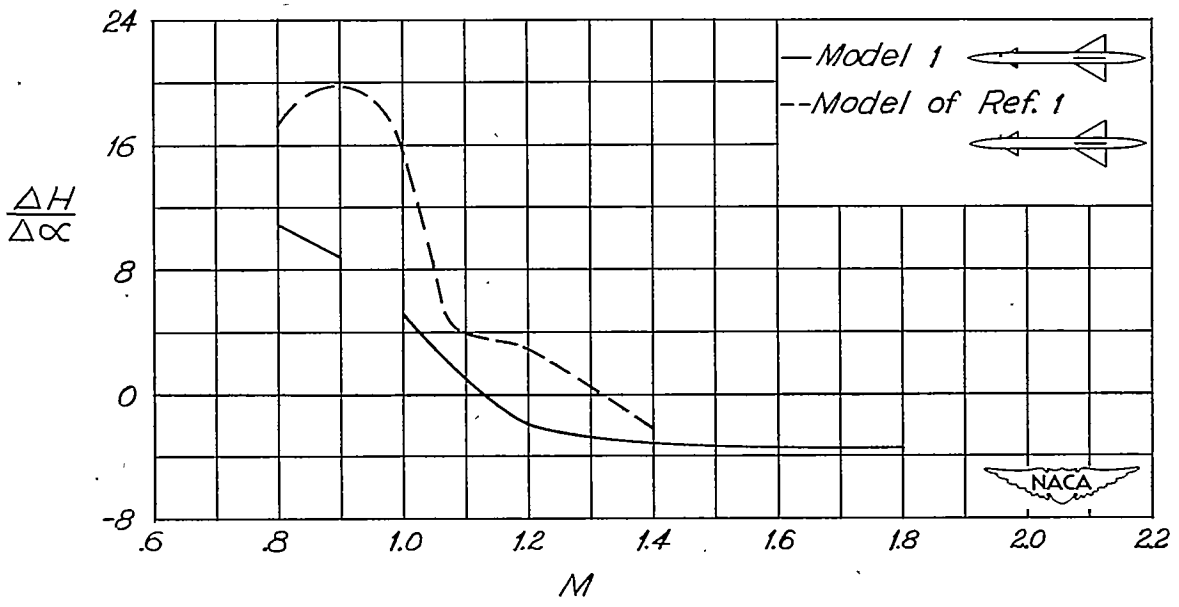

Figure 24.- Effect of canard area on total hinge moment required for trimmed flight.